

DS-K3DOM: 3-D Dynamic Occupancy Mapping with Kernel Inference and Dempster-Shafer Evidential Theory

Juyeop Han^{*1}, Youngjae Min^{*2}, Hyeok-Joo Chae¹, Byeong-Min Jeong¹ and Han-Lim Choi¹

Abstract—Occupancy mapping has been widely utilized to represent the surroundings for autonomous robots to perform tasks such as navigation and manipulation. While occupancy mapping in 2-D environments has been well-studied, there have been few approaches suitable for 3-D dynamic occupancy mapping which is essential for aerial robots. This paper presents a novel 3-D dynamic occupancy mapping algorithm called DS-K3DOM. We first establish a Bayesian method to sequentially update occupancy maps for a stream of measurements based on the random finite set theory. Then, we approximate it with particles in the Dempster-Shafer domain to enable real-time computation. Moreover, the algorithm applies kernel-based inference with Dirichlet basic belief assignment to enable dense mapping from sparse measurements. The efficacy of the proposed algorithm is demonstrated through simulations and real experiments¹.

I. INTRODUCTION

Understanding the surroundings is of great importance for autonomous robots deployed in unknown or partially known environments to perform tasks such as navigation and manipulation. One of the most central information about the surroundings is occupancy status for the area of interest to recognize target objects or find safe paths to destinations without any collisions. For these purposes, occupancy map is often employed by estimating whether each cell of discretized space or a point over continuous space is occupied by an object or not. When the occupying object is in motion, it is also essential to estimate its dynamic states such as velocity in addition to the occupancy to enable further missions such as collision avoidance and target tracking.

While occupancy mapping in two-dimensional (2-D) environments has been well-studied for ground vehicles, there have been few approaches suitable for 3-D dynamic occupancy mapping which is crucial for aerial robots. Prior to handling dynamic objects, occupancy mapping for static environments already introduces difficulty with sparse and noisy sensor measurements that cause inaccurate occupancy estimation. The problem is more severe in 3-D mapping compared to the 2-D cases as the same number of sensor rays results in sparser coverage in 3-D space. To resolve the issue, various studies have considered spatial correlation among

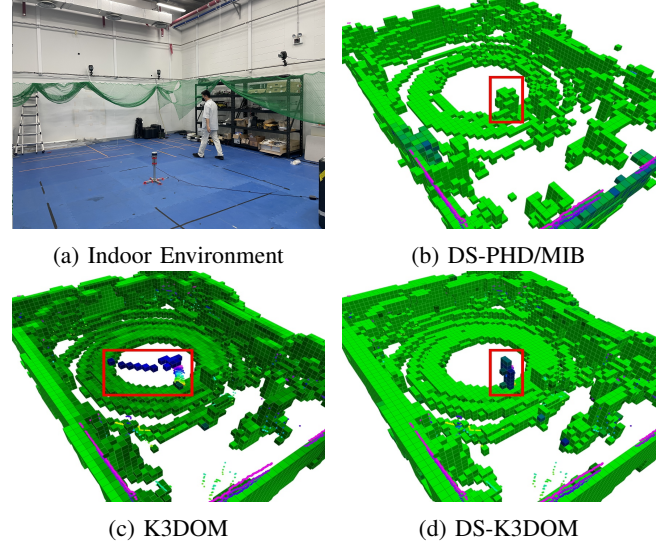


Fig. 1: Results of indoor experiments. (a) shows the environment in which a person walking around the LiDAR. (b-d) present the occupancy map estimated by each algorithm. They indicate estimated occupancy with different colors: blue and green for dynamic and static objects, respectively.

cells, for instance, using Gaussian process regression [1], logistic regression with hilbert maps [2], [3], and Bayesian kernel inference [4]. Nevertheless, they are incapable of updating the occupancy map along with the movements of dynamic objects and limited to static environments.

For dynamic environments, several methods have been proposed to accommodate dynamic objects by sequentially updating occupancy maps with a stream of measurements. [5], [6] proposed dynamic occupancy mapping in continuous space using Gaussian process regression, and [7] took a variational Bayesian approach on Hilbert mapping to learn occupancy maps sequentially. While these methods suffer from high computational cost, [8] proposed a real-time solution by employing a particle filter. [9], [10] also utilized particle filters in the Dempster-Shafer domain and showed satisfactory performance. Theoretically, [11] proposed a rigorous Bayesian method of occupancy mapping, called the PHD/MIB filter, based on the random finite set theory. Also, the authors presented its real-time viable approximation in the Dempster-Shafer domain with particles. However, those methods mainly target 2-D environments, and simply applying them to 3-D environments demands vast memory and computation capabilities due to the higher degree of

¹The authors are with the KAIST Institutes for Robotics and the Department of Aerospace Engineering, Korea Advanced Institute of Science and Technology (KAIST), Daejeon, 34141, South Korea {jyhan, bmjeong, hjchae}@lics.kaist.ac.kr, hanlimc@kaist.ac.kr

²Youngjae Min is with Laboratory for Information and Decision Systems (LIDS), Massachusetts Institute of Technology, Cambridge, MA 02139, USA yjm@mit.edu

^{*}equal contributions

¹The code is available at: https://github.com/JuyeopHan/dsk3dom_public

freedom of 3-D environments. Recently, [12] proposed a real-time solution for 3-D dynamic occupancy mapping, called K3DOM. It efficiently restricts the usage of particles on potential dynamic objects through a kernel-based inference on Dirichlet distribution. Nonetheless, the method is based on heuristics and lacks in rigorous foundation.

Inspired by the mathematical foundation of the PHD/MIB filter and the practicality of K3DOM, this paper presents a novel 3-D dynamic occupancy mapping algorithm called DS-K3DOM. We first theoretically extend the PHD/MIB filter to distinguish dynamic objects separately from static objects instead of treating them uniformly as occupying objects. Then, we approximate the extended PHD/MIB filter in the Dempster-Shafer domain with particles to enable real-time computation. Taking advantage of the extended structure, we employ particles efficiently to represent potential dynamic objects by proposing a kernel-based inference with Dirichlet basic belief assignment (BBA) [13]. The method also enables dense mapping from sparse measurements. The efficacy of the proposed algorithm is demonstrated through simulations and real experiments.

II. PRELIMINARIES

Before introducing the algorithm, we formulate the problem (II-A) and briefly review the concepts of random finite set (RFS) and probability hypothesis density (PHD) (II-B). For solid background, we refer the readers to [11], [14], [15].

A. Problem Formulation

This paper focuses on 3-D dynamic occupancy mapping in discrete space represented with cells. The main purpose of the problem is to estimate the occupancy state of each cell among $\Omega = \{D, S, F\}$ at each time-step where D, S, and F indicate the states occupied by dynamic objects, occupied by static objects, and not occupied (free), respectively. The ingredients for the state estimation at time-step k are accumulated range sensor measurements $Z_{1:k} := \{X_t, Y_t\}_{t=1}^k$ with measured location X_t and measured value Y_t at each time-step t . Y_t has a value of '0' or '1' denoting free or occupied measurement, respectively. Note that range sensors indirectly measure free space information. Thus, the closest point on each measurement ray from the query point is utilized as a free measurement as in [4].

B. Random Finite Set and Probability Hypothesis Density

An RFS $X = \{x_1, \dots, x_n\}$ is a random variable having a value as a finite set. The set consists of random vectors $x_i \in \mathbb{X}$ with a random cardinality n which follows the distribution $\rho(n) := P(|X| = n)$. A symmetric joint probability distribution function (PDF) of the elements of the RFS X is represented by $f_n(x_1, \dots, x_n)$ for $n > 0$. Then, the PDF of X , $\pi(X)$, and its integration are defined as below.

$$\pi(X = \{x_1, \dots, x_n\}) = n! \cdot \rho(n) \cdot f_n(x_1, \dots, x_n), \quad (1)$$

$$\int \pi(X) \delta X = \pi(\emptyset) + \sum_{n=1}^{\infty} \frac{1}{n!} \int \pi(\{x_1, \dots, x_n\}) dx_1 \cdots dx_n. \quad (2)$$

Note that $\pi(X = \emptyset) = \rho(0)$. Then, the PHD of the RFS X , $D(x)$, is defined over the state-space \mathbb{X} as

$$D(x) = E[\delta_X(x)] = \int \delta_X(x) \pi(X) \delta X, \quad (3)$$

where $\delta_X(x) := \sum_{s \in X} \delta_s(x)$ with a Dirac delta function $\delta_s(x)$ concentrated at each $s \in X$. Thus, the integration of $D(x)$ over an area represents the expected number of objects in the area.

III. EXTENDED PHD/MIB FILTER

In this section, we present the theoretical foundation of DS-K3DOM by extending the PHD/MIB filter [11]. The PHD/MIB filter represents a dynamic occupancy map with Bernoulli RFS and PHD. Assuming at most one object to exist in each cell, a Bernoulli RFS models the distribution of objects in each cell. Then, the PHD of the model characterizes the expected number of objects in a region via its integration. The filter then estimates the occupancy state of the map through the joint PHD of all Bernoulli RFSs. We extend this PHD/MIB filter to subdivide the feasible occupancy states of each cell into $\Omega = \{D, S, F\}$. Note that the original filter does not distinguish between the dynamic and static states and treats them uniformly as 'occupied'.

A. Representation of Objects via Bernoulli RFS and PHD

In our problem, each random vector $x = [p^T \ v^T]^T \in \mathbb{X}$ represents the state of a point object with its position $p \in \mathbb{R}^3$ and velocity $v \in \mathbb{R}^3$. For each cell (c) , let $r_D^{(c)}$ (resp. $r_S^{(c)}$) model the existence probability of any dynamic (resp. static) objects. Also, let $p_D^{(c)}(x)$ (resp. $p_S^{(c)}(x)$) denote the PDF of a dynamic (resp. static) object inside the cell. Then, under the assumption of having at most one object in each cell, the Bernoulli RFS of the cell is modeled to have PDF as

$$\pi^{(c)}(X) = \begin{cases} 1 - r^{(c)} & \text{if } X = \emptyset \\ r^{(c)} \cdot p^{(c)}(x) & \text{if } X = \{x\} \\ 0 & \text{if } |X| \geq 2 \end{cases} \quad (4)$$

with the existence probability $r^{(c)} = r_D^{(c)} + r_S^{(c)}$ and the PDF of an object inside the cell $p^{(c)}(x) = (r_D^{(c)} \cdot p_D^{(c)}(x) + r_S^{(c)} \cdot p_S^{(c)}(x)) / r^{(c)}$. Note that the PHD of the Bernoulli RFS is $D^{(c)}(x) = r^{(c)} \cdot p^{(c)}(x) = D_D^{(c)}(x) + D_S^{(c)}(x)$ if we consider the Bernoulli RFSs of dynamic and static objects with their PHDs $D_D^{(c)}(x) = r_D^{(c)} \cdot p_D^{(c)}(x)$ and $D_S^{(c)}(x) = r_S^{(c)} \cdot p_S^{(c)}(x)$, respectively. Thus, the extended filter separates the PHD of entire objects into those of dynamic and static objects.

B. Bayesian Update of Extended PHD/MIB Filter

The extended PHD/MIB filter updates the Bernoulli RFS and its PHD for new measurements in a Bayesian framework. It first predicts the future states by propagating the current estimation and then updates the prediction with new measurements to obtain the posterior estimation. Unlike the PHD/MIB filter, our extended filter utilizes the separated structures of the models for dynamic and static objects described in Section III-A.

In the prediction step, the movements of dynamic objects are the main source of change. Thus, we follow the standard prediction step of a PHD filter [16] for the dynamic portion, while the static portion remains the same. Representing the predicted joint PHD at time-step $k+1$ in the separated structure as $D_{+}(x_{k+1}) = D_{D+}(x_{k+1}) + D_{S+}(x_{k+1})$, each portion is predicted as:

$$\begin{aligned} D_{D+}(x_{k+1}) &= D_b(x_{k+1}) + p_S \int f_{D+}(x_{k+1}|x_k) D_D(x_k) dx_k, \\ D_{S+}(x_{k+1}) &= D_S(x_{k+1}), \end{aligned} \quad (5)$$

with the birth PHD $D_b(x_{k+1})$, the persistence probability p_S , and the transition density of a single dynamic object $f_{D+}(x_{k+1}|x_k)$. Here, we assume that the birth process only appears in dynamic states. We denote the last term in (5) as $D_{p,D+}(x_{k+1})$ to indicate the predicted PHD for persisting dynamic objects.

Next, we derive the Bernoulli RFSs corresponding to the predicted PHD. From the definition of PHD, the existence probabilities of the persistent dynamic objects and static objects in each cell (c) are, respectively,

$$r_{p,D+}^{(c)} = \min\left(\int_{x_{k+1} \in c} D_{p,D+}(x_{k+1}) dx_{k+1}, 1\right), \quad (7)$$

$$r_{S+}^{(c)} = \min(r_S^{(c)}, 1 - r_{p,D+}^{(c)}). \quad (8)$$

The probabilities are clipped so that each of them and their sum do not exceed 1. Meanwhile, the existence probability of new-born dynamic objects is modeled as

$$r_{b,D+}^{(c)} = p_B \cdot (1 - r_{p,D+}^{(c)} - r_{S+}^{(c)}), \quad (9)$$

given the prior birth probability p_B . Then, the PDF of the predicted objects inside the cell (c) is

$$p_{(\cdot)}^{(c)}(x_{k+1}) = D_{(\cdot)}(x_{k+1}) / r_{(\cdot)}^{(c)} \quad (10)$$

for nonzero $r_{(\cdot)}^{(c)}$ where (\cdot) corresponds to ‘ $b,D+$ ’, ‘ $p,D+$ ’, and ‘ $S+$ ’ for new-born dynamic, persistent dynamic, and static objects, respectively. With these parameters, the Bernoulli RFS of the entire objects in each cell (c) is predicted to have PDF

$$\begin{aligned} \pi_+^{(c)}(X_{k+1}) &= \\ &\begin{cases} 1 - r_{p,D+}^{(c)} - r_{b,D+}^{(c)} - r_{S+}^{(c)} & \text{if } X_{k+1} = \emptyset \\ r_{b,D+}^{(c)} p_{b,D+}^{(c)}(x_{k+1}) + r_{p,D+}^{(c)} p_{p,D+}^{(c)}(x_{k+1}) + r_{S+}^{(c)} p_{S+}^{(c)}(x_{k+1}) & \text{if } X_{k+1} = \{x_{k+1}\} \\ 0 & \text{if } |X_{k+1}| \geq 2 \end{cases} \end{aligned} \quad (11)$$

In the update step, the predicted PDF and new measurements Z_{k+1} are utilized to update the posterior PDF of Bernoulli RFS via the Bayes’ rule [15]:

$$\pi^{(c)}(X_{k+1}|Z_{k+1}) = \frac{\beta(Z_{k+1}|X_{k+1}) \pi_+^{(c)}(X_{k+1})}{\int \beta(Z_{k+1}|X_{k+1}) \pi_+^{(c)}(X_{k+1}) \delta X_{k+1}}, \quad (12)$$

where $\beta(Z_{k+1}|X_{k+1})$ denotes the likelihood function for the measurements Z_{k+1} given the posterior RFS X_{k+1} . We omit

the conditional part on the posterior for notational simplicity. Then, the joint posterior PHD of the map is given by the sum of all Bernoulli RFS instances in the map:

$$D_{k+1}(x_{k+1}) = \sum_c \pi^{(c)}(X_{k+1} = \{x_{k+1}\}). \quad (13)$$

IV. DS-K3DOM: APPROXIMATION OF EXTENDED PHD/MIB FILTER IN DEMPSTER-SHAFFER DOMAIN

In this section, we present DS-K3DOM by approximating the extended PHD/MIB filter in the Dempster-Shafer domain. By doing so, we enable real-time computation while theoretically computing the integrations in Section III-B is intractable in practice. We consider a particle realization in the Dempster-Shafer domain as in [11] for efficient use of particles. Alternatively, approximating the method in the Bayesian framework would induce particles unnecessarily distributed in the unobserved area. This hinders the algorithm to run in real time with an excessive number of particles required to estimate dynamic objects. We resolve this issue through a particle realization based on the Dempster-Shafer evidential theory (DST). Moreover, the DST provides a natural structure for the ambiguous sensor observations which do not distinguish between ‘dynamic (D)’ and ‘static (S)’. In the Dempster-Shafer domain, we also adopt Dirichlet BBA [13] to utilize a kernel-based inference, as in [12], for the sparse sensor measurements. The weight update and resampling processes for particles are the same with [11].

A. Dempster-Shafer Evidential Theory

We first briefly review the concept of the DST. For further knowledge, we refer the readers to [17]. Let a hypothesis be a possible and exclusive incident in a situation and a frame of discernment be the finite set Ω that consists of all possible hypotheses. A mapping called a basic belief assignment (BBA) or mass $m: 2^\Omega \rightarrow [0, 1]$ is defined to represent the normalized degree of evidence of a single hypothesis or a set of hypotheses, satisfying the conditions as below.

$$m(\emptyset) = 0 \text{ and } \sum_{X \subseteq \Omega} m(X) = 1 \quad (14)$$

A set X that satisfies $m(X) > 0$ is called a focal element. Dempster’s rule of combination is an operation that combines a pair of independent BBAs from multiple data sources that share the same frame of discernment Ω . The rule of combination is represented by

$$(m_1 \oplus m_2)(X) = \frac{\sum_{A \cap B = X} m(A)m(B)}{1 - \sum_{A \cap B = \emptyset} m(A)m(B)} \quad (15)$$

with $A, B, X \subseteq \Omega$.

B. Representation of Cell States in Dempster-Shafer Domain

In this paper, we assume that the sensor observations are from a range sensor. From the measurements, we only obtain an evidence that a cell is occupied or free. The BBAs $m(\{D, S\})$ and $m(\{F\})$ indicate the evidences supporting that the cell is occupied and free, respectively. The BBA of the state set itself $m(\Omega)$ indicates the degree of uncertainty of the cell state. Thus, the set of the focal elements Ξ is represented

as $\Xi = \{\{D\}, \{S\}, \{F\}, \{D, S\}, \Omega\}$. Based on the BBAs, we induce the pignistic probabilities [18] for the states of each cell (c) as

$$P^{(c)}(X) = \sum_{Y \in \Xi} \frac{|X \cap Y|}{|Y|} m(Y) \quad \forall X \in \Omega \quad (16)$$

Unlike [11], the sum of particle weights in each cell (c) represents the dynamic mass $m_k^{(c)}(\{D\})$, and the PDF of a dynamic point object $p_{D,k}^{(c)}(x_k)$ are approximated as below:

$$m_k^{(c)}(\{D\}) = \sum_{i=1}^{v_k^{(c)}} w_k^{(i,c)}, \quad (17)$$

$$p_{D,k}^{(c)}(x_k) \approx \frac{1}{m_k^{(c)}(\{D\})} \sum_{i=1}^{v_k^{(c)}} w_k^{(i,c)} \delta(x_k - x_k^{(i,c)}),$$

where $v_k^{(c)}$ indicates the number of particles of each cell (c) and $w_k^{(i,c)}$ is the weight of the i -th particle in the cell.

C. Prediction of Particles and Masses

We adopt a constant velocity (CV) model for the prediction step. The state of i -th persistent particle at the time-step $k+1$ is predicted to evolve as

$$x_{p,+} = \begin{bmatrix} I_3 & dt \cdot I_3 \\ \mathbf{0}_{3 \times 3} & I_3 \end{bmatrix} x_k + n_x \quad (18)$$

with a process noise $n_x = [n_p^T \ n_v^T]^T$, $n_p \sim N(\mathbf{0}_3, \sigma_p I_3)$, and $n_v \sim N(\mathbf{0}_3, \sigma_v I_3)$. As described in III-A, the first three dimensions are for position while the other three are for velocity.

The prediction of each focal element's mass is designed to imitate the prediction step in the extended PHD/MIB filter, (7-8), and to properly distribute $m_k^{(c)}(\{D, S\})$ to $m_{p,+}^{(c)}(\{D\})$ and $m_{p,+}^{(c)}(\{S\})$ as below:

$$\begin{aligned} m_{p,+}^{(c)}(\{D\}) &= \min \left(1, \sum_{i=1}^{v_{p,+}^{(c)}} w_{p,+}^{(i,c)} + \gamma^{dt} \alpha^{dt} \delta_k^{(c)} m_k^{(c)}(\{D, S\}) \right), \\ m_{p,+}^{(c)}(\{S\}) &= \min \left(1 - m_{p,+}^{(c)}(\{D\}), \right. \\ &\quad \left. \gamma^{dt} (m_k^{(c)}(\{S\}) + \alpha^{dt} (1 - \delta_k^{(c)}) m_k^{(c)}(\{D, S\})) \right), \\ m_{p,+}^{(c)}(\{D, S\}) &= \min \left(1 - m_{p,+}^{(c)}(\{D\}) - m_{p,+}^{(c)}(\{S\}), \right. \\ &\quad \left. \gamma^{dt} (1 - \alpha^{dt}) m_k^{(c)}(\{D, S\}) \right), \\ m_{p,+}^{(c)}(\{F\}) &= \min \left(1 - \text{bel}_{p,+}(\{D, S\}), \gamma^{dt} m_k^{(c)}(\{F\}) \right), \\ m_{p,+}^{(c)}(\Omega) &= 1 - \sum_{X \in 2^\Omega / \Omega} m_{p,+}^{(c)}(X). \end{aligned} \quad (19)$$

The factor α distributes the prior occupied mass $m_k^{(c)}(\{D, S\})$ to the dynamic mass $m_{p,+}^{(c)}(\{D\})$ and static mass $m_{p,+}^{(c)}(\{S\})$. $\delta_k^{(c)} := P_k^{(c)}(D) / (P_k^{(c)}(D) + P_k^{(c)}(S))$ is the distributing ratio for the dynamic mass, and the belief of the occupancy is $\text{bel}(\{D, S\}) := m(\{D\}) + m(\{S\}) + m(\{D, S\})$. γ denotes the decaying factor on the beliefs due to the increased

TABLE I: Parameters for Experiments

Parameter	Value
Cell edge size	0.2m
Number of consistent particles, v	2×10^6
Number of birth particles per step, v_b	2×10^5
SD process noise position, σ_p	0.05m
SD process noise velocity, σ_v	0.1m/s
Kernel length scale, l	0.5m
Kernel scale, σ_0	0.1
Persistence probability, p_s	0.99
Birth probability, p_b	0.02
Decaying factor, γ	0.99
Distributing factor, α	0.9
Sum of all Dirichlet priors, R_0	0.001

uncertainty with time. The condition (14) is satisfied by the minimum operations.

For every prediction step, the ratio of α^{dt} of decayed occupied mass $\gamma^{dt} m_k^{(c)}(\{D, S\})$ is assigned to $m_{p,+}^{(c)}(\{D\})$ and $m_{p,+}^{(c)}(\{S\})$. Specifically, the $\delta_k^{(c)}$ portion of the mass $\gamma^{dt} \alpha^{dt} m_k^{(c)}(\{D, S\})$ is assigned to $m_{p,+}^{(c)}(\{D\})$, and the rest is assigned to $m_{p,+}^{(c)}(\{S\})$. Since it is plausible to think that the mass of the occupied hypothesis $m_k^{(c)}(\{D, S\})$ is a potential for the dynamic or static states, we determine the portion $\delta_k^{(c)}$ in proportion to the probability of each state. The redistribution procedure is critical to spread out the occupied mass $m_k^{(c)}(\{D, S\})$ accumulated from the sensor observations since all particles are assigned only for the dynamic mass $m_k^{(c)}(\{D\})$.

D. Dirichlet BBA for Kernel Inference

We aim to generate a dense occupancy map by overcoming the sparse spatial density of range sensor measurements in the 3-D environment. We achieve this goal by inferring spatial information surrounding sensor observations using a kernel function as in [12]. However, the existing kernel inference is based on the Bayes' rule which cannot be applied in the Dempster-Shafer domain. Instead, we propose a new kernel inference using Dirichlet BBA [13] to combine the sensor information with the prior information by the rule of combination (15).

Let $\text{Dir}(\vec{\alpha})$ be the Dirichlet distribution of all focal elements of a frame of discernment Ω with the parameter vector $\vec{\alpha} = [\alpha(x_1), \dots, \alpha(x_n)]$ and focal elements $x_1, \dots, x_n \in \Xi$. Each element of the vector $\alpha(x_i)$ is a sum of a prior evidence $r_0(x_i)$ and an observation evidence $r(x_i)$, and R_0 denotes the sum of all prior evidence:

$$\alpha(x_i) = r_0(x_i) + r(x_i) \quad \text{and} \quad R_0 = \sum_{X_i \in \Xi} r_0(X_i) \quad (20)$$

We now define BBAs of focal elements based on the parameters satisfying the conditions for BBA (14) as below:

$$m(x_i) = \begin{cases} r(x_i) / \sum_{x_j \in \Xi} \alpha(x_j) & \text{if } x_i \in \Xi / \{\Omega\} \\ R_0 / \sum_{x_j \in \Xi} \alpha(x_j) & \text{if } x_i = \Omega \end{cases} \quad (21)$$

We build an observation BBA $m_{Z_{k+1}}^{(c)}$ using (21) with a set of sensor measurements $Z_{k+1} = \{X_{k+1}, Y_{k+1}\}$. Kernel inference is introduced by updating observation evidence of

the occupied and free measurement, $r(\{D, S\})$ and $r(\{F\})$, respectively given a query point x_* :

$$\begin{aligned} r(\{D, S\}) &= \sum_{(x,y) \in \{X,Y\}} k(x_*, x)y \\ r(\{F\}) &= \sum_{(x,y) \in \{X,Y\}} k(x_*, x)(1-y) \end{aligned} \quad (22)$$

Note that $r(x) = 0$ if $x \neq \{D, S\}$ or $x \neq \{F\}$. The kernel function $k(x, x')$ is employed as [4] and [12]:

$$k(x, x') := \begin{cases} \sigma_0 [\frac{1}{3}(2 + \cos(2\pi \frac{d}{l}))(1 - \frac{d}{l}) + \frac{1}{2\pi} \sin(2\pi \frac{d}{l})] & \text{if } d < l \\ 0 & \text{if } d \geq l \end{cases} \quad (23)$$

with $d := \|x - x'\|_2$, a kernel scale σ_0 , and a length scale l .

E. Update of BBA and mass of the Birth Dynamic Object

The posterior BBA is generated by combining the predicted BBA $m_{p,+}^{(c)}$ and the observation BBA $m_{Z_{k+1}}^{(c)}$ with the rule of combination (15):

$$m_{k+1}^{(c)} = m_{p,+}^{(c)} \oplus m_{Z_{k+1}}^{(c)} \quad (24)$$

The dynamic mass $m_{k+1}^{(c)}(D)$ is divided by the persistent dynamic object mass $\rho_{p,k+1}^{(c)}$ and the birth dynamic object mass $\rho_{b,k+1}^{(c)}$, i.e. $m_{k+1}^{(c)}(D) = \rho_{p,k+1}^{(c)} + \rho_{b,k+1}^{(c)}$.

Assume that posterior probabilities of a persistent and a birth dynamic object in the extended PHD/MIB filter, $r_{p,D,k+1}$ and $r_{b,D,k+1}$, are the same as corresponding predicted probabilities, $r_{p,D,+}$ and $r_{b,D,+}$ as [11]. By considering (9), the ratio between the two posterior probabilities are

$$\frac{r_{b,k+1}^{(c)}}{r_{p,k+1}^{(c)}} = \frac{r_{b,+}^{(c)}}{r_{p,+}^{(c)}} = \frac{p_B(1 - r_{p,D,+}^{(c)} - r_{S,+}^{(c)})}{r_{p,+}^{(c)}}. \quad (25)$$

We set the ratio between $\rho_{p,k+1}^{(c)}$ and $\rho_{b,k+1}^{(c)}$ similar to (25):

$$\frac{\rho_{b,k+1}^{(c)}}{\rho_{p,k+1}^{(c)}} = \frac{p_B(1 - m_{p,+}^{(c)}(D) - m_{p,+}^{(c)}(S))}{m_{p,+}^{(c)}(D)} \quad (26)$$

Therefore, the posterior dynamic masses, $\rho_{p,k+1}^{(c)}$ and $\rho_{b,k+1}^{(c)}$, are derived as:

$$\begin{aligned} \rho_{b,k+1}^{(c)} &= \frac{m_{k+1}^{(c)}(D) \cdot p_B(1 - m_{p,+}^{(c)}(D) - m_{p,+}^{(c)}(S))}{p_B(1 - m_{p,+}^{(c)}(D) - m_{p,+}^{(c)}(S)) + m_{p,+}^{(c)}(D)} \\ \rho_{p,k+1}^{(c)} &= m_{k+1}^{(c)}(D) - \rho_{b,k+1}^{(c)} \end{aligned} \quad (27)$$

V. EXPERIMENTS

A. Setup

We evaluate the performance of DS-K3DOM through simulation and indoor experiments, comparing it with that of baselines, DS-PHD/MIB filter [11] and K3DOM [12]. The DS-PHD/MIB filter is extended from the 2D to the 3D domain for experiments. The algorithms are implemented in

ROS *Melodic* using CUDA parallel computing. The simulation is conducted in *Gazebo* with a desktop installed in Intel Core i7-8700 hexa-core CPU and RTX 3060 Ti. A VLP-16 model of *veolodyne_simulator* package is adopted as a virtual LiDAR model. Table I shows values of parameters used in the two experiments. The edge of the local map is set to 40m and 15m for simulation and indoor experiments, respectively. For more information on parameters used in the baselines, we refer the reader to [11] and [12].

The simulation is designed to evaluate the performance for classification and velocity estimation of each algorithm. The simulation environment contains static and dynamic objects. Static obstacles consist of four brick buildings. An ego vehicle with a LiDAR sensor and dynamic objects, named 'Box 0', 'Box 1', and 'Cylinder 0', keep moving through the intersection road as shown in Fig. 2a.

We assess the classification performance for the 'occupied (O)' and 'dynamic (D)' of each algorithm by evaluating cells corresponding to static objects and dynamic objects. The classification standards for DS-PHD/MIB filter and K3DOM are described in [12]. At the first step, insufficiently observed cells are filtered out if

$$\zeta_0 < m^{(c)}(\Omega) \quad (28)$$

The parameters, ζ_0 , are empirically set to $\zeta_0 = 0.5$. The cell is classified as 'O' or 'D' if

$$\begin{cases} P^{(c)}(D) + P^{(c)}(S) > \zeta_1 & \text{for 'O'} \\ P^{(c)}(D) > \zeta_2 & \text{for 'D'} \end{cases} \quad (29)$$

The cell is correctly classified as (i) 'O' if any objects contain the cell (ii) 'D' if the dynamic objects contain the cell. $P^{(c)}(\cdot)$ is a pignistic probability in (16). We obtain ROC (Receiver Operating Characteristic) curves and their AUC (Area Under Curve) by changing parameters ζ_1 and ζ_2 .

The velocity of each dynamic object for DS-K3DOM is estimated as an average of velocities of all cells contained in the object, (30). The velocity of the dynamic object for the baselines is estimated in the same way of [12] as well. The magnitude of error velocity obtained by each algorithm are compared with each other.

$$v_{obj} = \frac{\sum_{c \in obj} v^{(c)} \rho_p^{(c)}}{\sum_{c \in obj} \rho_p^{(c)}} \quad (30)$$

In the indoor experiment, the VLP-16 LiDAR is separated from the ground and is fixed by a support, and a person walks around the LiDAR as Fig. 1a shows. A Jetson AGX Xavier connected to the VLP-16 LiDAR collects point cloud data. The performance of each algorithm is qualitatively assessed in the indoor experiment.

B. Simulation

As shown in Fig. 2d, 'D' cells exist on the ground since DS-K3DOM falsely recognizes that the point clouds on the ground is moving contrary to the fact that the sensor is moving. Therefore, we implement an additional DS-K3DOM

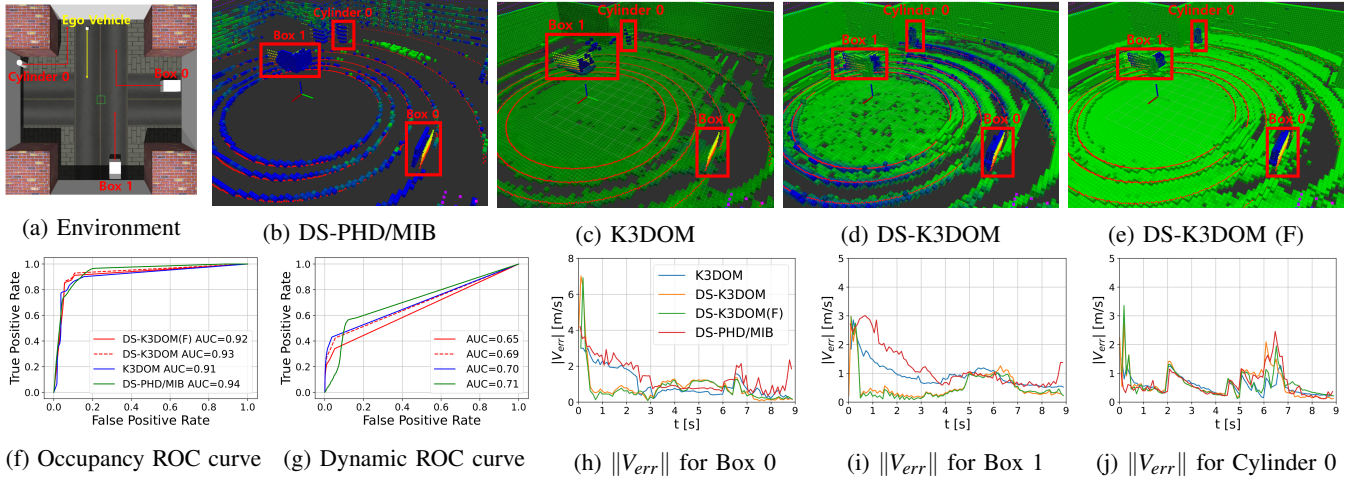


Fig. 2: Environment and results of simulation experiment. (a) shows *Gazebo* simulation environment. (b-e) represent occupancy map of each algorithm. In (b-e), Colored dots indicate point clouds, Green cells represent 'static (S)' state cells, and Blue color of cells represents 'dynamic (D)' cells. (f-g) denote ROC curves of cell state classification (h-j) graph error magnitudes between the true velocity and the estimated velocity for each dynamic object.

algorithm, called 'DS-K3DOM (F)', by removing particles on the ground to remove 'D' cells on the ground as Fig. 2e.

In Fig. 2b - 2e, DS-K3DOM and DS-K3DOM (F) produce an occupancy map much more densely than baselines. Particularly, DS-PHD/MIB filter generates the most sparse occupancy map than the other algorithms as shown in Fig. 2b. Moreover, DS-PHD/MIB filter classifies many parts of static objects as 'D', while the other algorithms classify static objects in the right way. Dynamic objects are not effectively shown as cells by the baselines. For example, in Fig. 2b - 2c, 'Box 1' and 'Cylinder 0' are represented as the insufficient number of cells. Even worse, 'Box 0' is invisible, and there are trail noise cells near 'Box 1' in K3DOM. Unlike the baselines, the proposed algorithms densely represent dynamic objects as shown in Fig. 2d - 2e.

In Fig. 2f, all algorithms show high classification performance for the 'O' state. The high AUCs of DS-K3DOM and DS-K3DOM (F) show that the algorithms are sufficient to classify the 'O' state although these AUCs are slightly lower than those of baselines. It seems that the baselines classify 'D' cells slightly better than the others in Fig. 2g. However, the seemingly better performance is due to the fact that the dynamic objects are expressed as only the sparse number of 'D' cells in baselines although the dynamic objects are expressed as the dense number of 'D' and 'S' cells in the proposed algorithms. In other words, Fig. 2g does not imply that the baselines have a better performance for detecting dynamic objects than the others.

Fig. 2h-2j show that the estimated velocity for DS-K3DOM and DS-K3DOM (F) converges to the true velocity much faster than that for the baselines and that the magnitude of the error velocity for the proposed algorithms is lower than that for the baselines during most of the time.

The proposed algorithms are implemented in real time in the experiment, whose processing time is about 4.5Hz.

C. Indoor Experiment

The red boxes in Fig. 1b - 1d denote point the person walking around the LiDAR. In Fig. 1b, DS-PHD/MIB filter represents the person as 'S' cells. As Fig. 1c shows, K3DOM produces trail noise of the person, unlike DS-K3DOM. As shown in Fig. 1b - 1d, DS-K3DOM generates a much denser occupancy map. Also, DS-K3DOM showed real-time capability. It was processed in about 7.5Hz and 6Hz on the desktop and the Jetson Xavier respectively throughout the indoor experiment.

VI. CONCLUSION

In the paper, a novel 3-D dynamic occupancy mapping algorithm, DS-K3DOM, was proposed by mathematically extending PHD/MIB filter and applying kernel inference with Dirichlet BBA to build a dense occupancy map from sparse measurements. Experiments have verified that DS-K3DOM shows higher performances for dense mapping and velocity estimation compared to baselines, with a real time implementation. The limitation of the research is that DS-K3DOM falsely represents some part of a large dynamic object as static cells. Future works may include heterogeneous sensor fusion or theoretical improvement for achieving a better performance.

ACKNOWLEDGMENT

This research was supported by Unmanned Vehicles Core Technology Research and Development Program through the National Research Foundation of Korea(NRF), Unmanned Vehicle Advanced Research Center(UVARC) funded by the Ministry of Science and ICT, the Republic of Korea (2020M3C1C1A01082375)

REFERENCES

- [1] Simon T O'Callaghan and Fabio T Ramos. Gaussian process occupancy maps. *The International Journal of Robotics Research*, 31(1):42-62, 2012.

- [2] Kevin Doherty, Jinkun Wang, and Brendan Englot. Probabilistic map fusion for fast, incremental occupancy mapping with 3d hilbert maps. In *2016 IEEE international conference on robotics and automation (ICRA)*, pages 1011–1018. IEEE, 2016.
- [3] Fabio Ramos and Lionel Ott. Hilbert maps: Scalable continuous occupancy mapping with stochastic gradient descent. *The International Journal of Robotics Research*, 35(14):1717–1730, 2016.
- [4] Kevin Doherty, Tixiao Shan, Jinkun Wang, and Brendan Englot. Learning-aided 3-d occupancy mapping with bayesian generalized kernel inference. *IEEE Transactions on Robotics*, 35(4):953–966, 2019.
- [5] Simon T O’Callaghan and Fabio T Ramos. Gaussian process occupancy maps for dynamic environments. In *Experimental Robotics*, pages 791–805. Springer, 2016.
- [6] Ransalu Senanayake, Simon O’Callaghan, and Fabio Ramos. Learning highly dynamic environments with stochastic variational inference. In *2017 IEEE International Conference on Robotics and Automation (ICRA)*, pages 2532–2539. IEEE, 2017.
- [7] Ransalu Senanayake and Fabio Ramos. Bayesian hilbert maps for dynamic continuous occupancy mapping. In *Conference on Robot Learning*, pages 458–471. PMLR, 2017.
- [8] Radu Danescu, Florin Oniga, and Sergiu Nedevschi. Modeling and tracking the driving environment with a particle-based occupancy grid. *IEEE Transactions on Intelligent Transportation Systems*, 12(4):1331–1342, 2011.
- [9] Georg Tanzmeister and Dirk Wollherr. Evidential grid-based tracking and mapping. *IEEE Transactions on Intelligent Transportation Systems*, 18(6):1454–1467, 2016.
- [10] Sascha Steyer, Georg Tanzmeister, and Dirk Wollherr. Grid-based environment estimation using evidential mapping and particle tracking. *IEEE Transactions on Intelligent Vehicles*, 3(3):384–396, 2018.
- [11] Dominik Nuss, Stephan Reuter, Markus Thom, Ting Yuan, Gunther Krehl, Michael Maile, Axel Gern, and Klaus Dietmayer. A random finite set approach for dynamic occupancy grid maps with real-time application. *The International Journal of Robotics Research*, 37(8):841–866, 2018.
- [12] Youngjae Min, Do-Un Kim, and Han-Lim Choi. Kernel-based 3-d dynamic occupancy mapping with particle tracking. In *2021 IEEE International Conference on Robotics and Automation (ICRA)*, pages 5268–5274, 2021.
- [13] Audun Jøsang and Zied Elouedi. Interpreting belief functions as dirichlet distributions. In Khaled Mellouli, editor, *Symbolic and Quantitative Approaches to Reasoning with Uncertainty*, pages 393–404, Berlin, Heidelberg, 2007. Springer Berlin Heidelberg.
- [14] Ronald P. S. Mahler. *Statistical Multisource-Multitarget Information Fusion*. Artech House, Inc., USA, 2007.
- [15] Branko Ristic, Michael Beard, and Claudio Fantacci. An overview of particle methods for random finite set models. *Information Fusion*, 31:110–126, 2016.
- [16] R.P.S. Mahler. Multitarget bayes filtering via first-order multitarget moments. *IEEE Transactions on Aerospace and Electronic Systems*, 39(4):1152–1178, 2003.
- [17] Uwe Kay Rakowsky. Fundamentals of the dempster-shafer theory and its applications to reliability modeling. *International Journal of Reliability, Quality and Safety Engineering*, 14(6):579–601, 2007.
- [18] P. Smets. Data fusion in the transferable belief model. In *Proceedings of the Third International Conference on Information Fusion*, volume 1, pages PS21–PS33 vol.1, 2000.